Broad-band negative refraction via simultaneous multi-electron transitions

Journal of Physics Communications

OPEN ACCESS

RECEIVED
20 September 2018

REVISED
27 December 2018

ACCEPTED FOR PUBLICATION
14 January 2019

PUBLISHED
23 January 2019

PAPER

Broad-band negative refraction via simultaneous multi-electron transitions

Jing-Jing Cheng[1,4], Ying-Qi Chu[1,4], Tao Liu[2], Jie-Xing Zhao[1], Fu-Guo Deng[1], Qing Ai[1,5] and Franco Nori[2,3,5]

[1] Department of Physics, Applied Optics Beijing Area Major Laboratory, Beijing Normal University, Beijing 100875, People's Republic of China
[2] Theoretical Quantum Physics Laboratory, RIKEN Cluster for Pioneering Research, Wako-shi, Saitama 351-0198, Japan
[3] Department of Physics, The University of Michigan, Ann Arbor, Michigan 48109-1040, United States of America
[4] J.-J.C. and Y.-Q.C. contributed equally to this work.
[5] Authors to whom any correspondence should be addressed.

E-mail: aiqing@bnu.edu.cn and fnori@riken.jp

Keywords: metamaterials, multi-electron transitions, NV centers

Abstract

The potential applications of metamaterials with negative refraction are limited by their narrow bandwidth and difficulty in fabrication. In order to broaden the bandwidth, we analyze different factors which influence the negative refraction in solids and multi-atom molecules. We find that this negative refraction can be significantly enhanced by simultaneous multi-electron transitions with the same transition frequency and dipole redistribution over different eigenstates. We show that these simultaneous multi-electron transitions and enhanced transition dipole *broaden* the bandwidth of the negative refraction by at least *one order of magnitude*. Furthermore, we show the possible application of this scheme in hyperbolic metamaterials using diamonds with NV centers.

1. Introduction

Metamaterials with negative refraction [1–7] have attracted broad interest because of their potential applications, including perfect lenses [2, 8], fingerprint identification in forensic science [9], simulating condensed matter phenomena and reversed Doppler effect [10, 11], controlling light polarization [12], and electromagnetic cloaking [13–15]. In order to realize metamaterials, a number of routes have been proposed, including (molecular) split-ring resonators [3, 16, 17], chiral approaches [18], hyperbolic dispersion [19–22], dark-state mechanism [23–27], and topological routes [28–30]. However, none of these can effectively overcome the difficulty of realizing broad-band negative refraction.

Generally, it is expensive to fabricate optical metamaterials, as most of these require producing a huge number of split-ring resonators, which are of sub-optical-wavelength. Also, the size of a resonator in classical metamaterials is of the order of the sub-wavelength of the electromagnetic field [31, 32]. However, since in a molecular medium the electromagnetic response results from quantum transitions, the size of a molecule can be intrinsically smaller by 2 orders of magnitude than the size of a resonator for classical metamaterials. Furthermore, molecular media are crystals of such molecules and thus can be easily fabricated by crystallization. Therefore, these observations motivate us to consider fabricating metamaterials using chemical molecules.

In multi-atom molecules and solids, there are generally more than one electron which can respond to applied electromagnetic fields. In previous investigations [9, 17, 23–25, 30, 33–38], only transitions for a *single* electron were considered. Because each atom contributes a π-electron to the molecule, there are N π-electrons in a molecule with N atoms. Thus, there would be N possible transitions for the π-electrons in the molecule. Since two or more transitions can effectively overlap with each other, it would be reasonable to expect a broadened bandwidth of the negative refraction by simultaneous multi-electron transitions. On the other hand, Möbius molecules with nontrivial topology have been synthesized [39–43] and proposed to realize, e.g., metamaterials

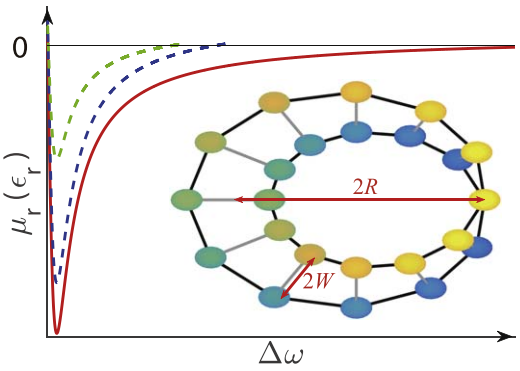

Figure 1. Schematic illustration of broad-band negative refraction induced by simultaneous multi-electron transitions. Dashed curves are for single-electron transitions, while the solid curve provides the overall simultaneous contribution. Inset: Top view of a Möbius molecule with $N = 12$ carbon atoms in each ring. The adjacent atoms are linked with covalent bonds.

[28, 30, 44], quantum devices [45–47], dual-mode resonators and bandpass filters [48], topological insulators [49], molecular knots and engines [50], and artificial light harvesting [51, 52].

As a concrete example for demonstrating the above principle, here we consider multi-electron transitions in a double-ring Möbius molecule [30, 47] with $2N$ π-electrons. Every energy level could be filled with two electrons of different spins, due to Pauli's exclusion principle. Because the lower energy level has a higher probability to be filled with electrons, half of the N energy levels with lower energy can be filled. Furthermore, electrons can transit from a highest occupied molecular orbital (HOMO) to a lowest unoccupied molecular orbital (LUMO). Because multi-electrons can be involved in the transitions of nearby frequencies, the bandwidth of the negative refraction would be *significantly broadened* compared to previous findings [23, 24, 30, 34, 36], as schematically illustrated in figure 1.

This paper is organized as follows: In the next section, we briefly introduce the relative permittivity and permeability for simultaneous multi-electron transitions by linear-response theory. In section 3, we summarize the selection rules for optical transitions in Möbius molecules from the transition matrices of electric and magnetic dipoles, as given in appendix A. Then, we show the significantly-broadened bandwidths of the negative refraction by simultaneous multi-electron transitions in section 4. Finally, the main results are summarized in section 5.

2. Simultaneous multi-electron transitions

The electric displacement field $\vec{D}$ and magnetic induction $\vec{B}$ can be written as [31, 32]

$$\vec{D} = \varepsilon_0 \vec{E} + \vec{P} = \varepsilon_0 \overleftrightarrow{\varepsilon}_r \vec{E}, \tag{1}$$

$$\vec{B} = \mu_0 (\vec{H} + \vec{M}) = \mu_0 \overleftrightarrow{\mu}_r \vec{H}, \tag{2}$$

where $\vec{E}$ is the applied electric field, $\vec{P}$ is the polarization, ε_0 and $\varepsilon_0 \overleftrightarrow{\varepsilon}_r$ are, respectively, the permittivity of the vacuum and medium, $\vec{H}$ is the applied magnetic field, $\vec{M}$ is the magnetization, μ_0 and $\mu_0 \overleftrightarrow{\mu}_r$ are, respectively, the permeability of the vacuum and medium. In order to simulate the electromagnetic response of the Möbius medium in the presence of applied fields, we employ linear-response theory [53] to calculate the electric permittivity and magnetic permeability. When there is an electric field applied on the Möbius molecule, the molecule is polarized as

$$\langle \vec{d} \rangle = \int \frac{d\omega}{2\pi} S(\omega) \vec{E}(\omega) e^{-i\omega t}, \tag{3}$$

where

$$\vec{E}(\omega) = \int_{-\infty}^{\infty} dt\ \vec{E}(t) e^{i\omega t} \tag{4}$$

is the Fourier transform of the time-dependent electric field

$$\vec{E}(t) = \vec{E}_0 \cos \omega t, \tag{5}$$

with amplitude $\vec{E}_0$ and frequency ω,

$$S(\omega) = -J(\omega) - J^*(-\omega). \tag{6}$$

Here, the dipole-dipole correlation function reads

$$J(\omega) = -i\int_0^\infty dt\ \mathrm{Tr}\,[\vec{d}(t)\vec{d}\rho(0)]e^{i\omega t}, \tag{7}$$

where $\rho(0)$ is the initial state of the molecule.

Because of the dipole approximation [31, 32], the molecular electric dipole can be calculated as

$$\langle \vec{d}\ \rangle \approx -\sum_{i,f}\mathrm{Re}\left[\frac{\vec{d}_{if}\vec{d}_{fi}\cdot\vec{E}(t)}{n_i\hbar(\omega-\Delta_{fi}+i\gamma)}\right], \tag{8}$$

where $\vec{d}_{if}$ is the transition electric dipole between the initial state $|i\rangle$ and the final state $|f\rangle$ with level spacing $\hbar\Delta_{fi}$, n_i^{-1} is the number of electrons occupying the initial state, $\hbar$ is the Planck constant. Here, we phenomenologically introduce the decay rate γ to describe the decoherence effects on the excited states. This is equivalent to approximately solving the master equation by the quantum jump approach when the decoherence effects are much slower than the typical frequency of the system Hamiltonian [54, 55]. In a similar way, the molecular magnetic dipole is calculated as

$$\langle \vec{m}\ \rangle \approx -\sum_{i,f}\mathrm{Re}\left[\frac{\vec{m}_{if}\vec{m}_{fi}\cdot\vec{H}(t)}{n_i\hbar(\omega-\Delta_{fi}+i\gamma)}\right], \tag{9}$$

where $\vec{m}_{if}$ is the transition magnetic dipole between the initial state $|i\rangle$ and the final state $|f\rangle$, $\vec{H}$ is the applied magnetic field. Under the dipole approximation, according to linear-response theory [53], the relative permittivity and permeability are given by [9, 17, 22–25, 30]

$$\overleftrightarrow{\varepsilon}_r = 1 - \sum_{i\neq f}\frac{\vec{d}_{if}\vec{d}_{fi}}{n_i\hbar\varepsilon_0 v_0}\mathrm{Re}\left(\frac{1}{\omega-\Delta_{fi}+i\gamma}\right), \tag{10}$$

$$\overleftrightarrow{\mu}_r = 1 - \sum_{i\neq f}\frac{\mu_0\vec{m}_{if}\vec{m}_{fi}}{n_i\hbar v_0}\mathrm{Re}\left(\frac{1}{\omega-\Delta_{fi}+i\gamma}\right), \tag{11}$$

where v_0 is the volume of the molecule.

In obtaining (10), (11), we assume that all molecules are identical, and every molecule responds equally to the applied electromagnetic field. Due to the response of the molecules, the actual electromagnetic field inside the medium is different from that in the vacuum. However, it can be proven by Lorentzian local-field theory that both the center and bandwidth of the negative refraction will not be modified significantly [22–24, 30]. Only the magnitudes of permittivity and permeability are significantly modified. Furthermore, the dipole-dipole interaction between molecules can be omitted as long as it is smaller than either the decoherence rate of the molecular excited states [56, 57] or the static disorder [58].

3. Selection rules for transitions

As a specific case, we consider a Möbius molecule with double rings consisting of $2N$ carbon atoms [41], as shown in figure 1. The jth atomic position of ring a (b) is $\vec{R}_{j+}$ ($\vec{R}_{j-}$) with

$$\vec{R}_{j\pm} = \left(R \pm W\sin\frac{\varphi_j}{2}\right)\cos\varphi_j\hat{e}_x \pm W\cos\frac{\varphi_j}{2}\hat{e}_z + \left(R \pm W\sin\frac{\varphi_j}{2}\right)\sin\varphi_j\hat{e}_y, \tag{12}$$

where the radius and width of the Möbius molecule are, respectively, R and $2W$, with W the radius of the carbon atom, $\varphi_j = j\delta$, and $\delta = 2\pi/N$. According to the Hückel molecular orbital theory [59], the Hamiltonian of the Möbius molecule for the single electron is [30, 47]

$$H = \sum_{j=0}^{N-1}[A_j^\dagger MA_j - \xi(A_j^\dagger A_{j+1} + \mathrm{h.c.})], \tag{13}$$

where $A_j = (a_j, b_j)^T$ with a_j (b_j) the annihilation operator at the jth site of ring a (b),

$$M = \begin{bmatrix}\epsilon & -V\\ -V & -\epsilon\end{bmatrix}, \tag{14}$$

ϵ is the on-site energy difference between the two rings, and $V(\xi)$ is the inter-ring (intra-ring) resonant integral. Because of the Möbius boundary condition, the last atom of each ring is linked to the first atom of the other ring, i.e. $a_0 = b_N$, and $b_0 = a_N$.

The Möbius boundary condition can be canceled by a local unitary transformation, i.e. $B_j \equiv (c_{j\uparrow}, c_{j\downarrow})^T = U_jA_j$, $B_N = B_0$, where $c_{j\sigma}$ is the annihilation operator of an electron at jth atomic site with σ pseudo-spin label,

$$U_j = \frac{1}{\sqrt{2}}\begin{bmatrix} e^{-i\varphi_j/2} & -e^{-i\varphi_j/2} \\ 1 & 1 \end{bmatrix}. \tag{15}$$

Therefore, the Hamiltonian with periodic boundary condition can be rewritten as

$$H = \sum_{j=0}^{N-1} [B_j^\dagger V\sigma_z B_j - \xi(B_j^\dagger Q B_{j+1} + \text{h.c.})], \tag{16}$$

where

$$Q = \begin{bmatrix} e^{i\delta/2} & 0 \\ 0 & 1 \end{bmatrix}. \tag{17}$$

By using the Fourier transformation, $B_j = \sum_k e^{-ikj} C_k$, the Hamiltonian of the Möbius molecule is diagonalized as

$$H = C_k^\dagger E_k C_k, \tag{18}$$

where $C_k = (c_{k\uparrow}, c_{k\downarrow})^T$ with

$$c_{k\uparrow} = \frac{1}{\sqrt{2N}} \sum_{j=0}^{N-1} e^{-i(k-\delta/2)j}(a_j^\dagger - b_j^\dagger), \tag{19}$$

$$c_{k\downarrow} = \frac{1}{\sqrt{2N}} \sum_{j=0}^{N-1} e^{-ikj}(a_j^\dagger + b_j^\dagger), \tag{20}$$

$$E_k = \begin{bmatrix} E_{k\uparrow} & 0 \\ 0 & E_{k\downarrow} \end{bmatrix} \tag{21}$$

with $E_{k\uparrow} = V - 2\xi\cos\left(k - \frac{\delta}{2}\right)$ and $E_{k\downarrow} = -V - 2\xi\cos k$ the eigenenergies of the upper and lower bands, respectively.

In (10), (11), we apply linear-response theory to rewrite the relative permittivity and permeability in terms of the transition matrix elements of the electric and magnetic dipoles, i.e. $\vec{d}_{if}$ and $\vec{m}_{if}$. According to (10), (11), we would expect negative permittivity and permeability close to the transition frequencies $\Delta_{fi} = (E_f - E_i)/\hbar$. The selection rules of transitions are explicitly provided by the matrix elements of the electric and magnetic dipoles as given in appendix A.

Using the dipole approximation, the interaction Hamiltonian with the electric field is written as [31, 32]

$$H_E' = -\vec{d}\cdot\vec{E}_0\cos\omega t, \tag{22}$$

where the molecule is subject to an electric field with amplitude $\vec{E}_0 = (E_0^x, E_0^y, E_0^z)$ and frequency ω. The electric-dipole-induced transition is allowed if the corresponding matrix element is nonzero. By using the relation $\langle\phi_{js}|\vec{r}|\phi_{j's'}\rangle = \vec{R}_{js}\delta_{jj'}\delta_{ss'}$ [59], the selection rules for the electric-dipole-induced transitions are summarized as

$$|k,\downarrow\rangle \overset{x,y,z}{\rightleftharpoons} |k,\uparrow\rangle, \tag{23a}$$

$$|k,\downarrow\rangle \overset{x,y}{\rightleftharpoons} |k+2\delta,\uparrow\rangle, \tag{23b}$$

$$|k,\downarrow\rangle \overset{x,y,z}{\rightleftharpoons} |k+\delta,\uparrow\rangle, \tag{23c}$$

$$|k,\downarrow\rangle \overset{x,y}{\rightleftharpoons} |k-\delta,\uparrow\rangle, \tag{23d}$$

where the superscripts over the arrows indicate the polarizations of the electric fields. In the following calculations, we only consider the transitions from the lower band to the upper band because of the rotating-wave approximation [60, 61] and initial condition. However, it has been shown that the counter-rotating terms will essentially influence the quantum dynamics in combination with some specific initial states [60, 62]. Here, we remark that when the temperature is sufficiently high or the initial state is prepared on purpose, the transition from the upper band to the lower band will also participate in the response of metamaterials to the applied electromagnetic fields. Under the dipole approximation, the interaction Hamiltonian with the magnetic field is written as [31, 32]

$$H_B' = -\vec{m}\cdot\vec{B}_0\cos\omega t, \tag{24}$$

where $\vec{B}_0 = (B_0^x, B_0^y, B_0^z)$. A straightforward calculation in appendix A shows that the selection rules for the magnetic-dipole-induced transitions are the same as (3).

The transitions allowed by both electric and magnetic dipole couplings are depicted in figure 2, in combination with initial and final conditions. Because a transition can take place from the HOMOs, denoted by solid symbols, to the LUMOs, denoted by empty symbols. The initial state $|i\rangle$ of the molecule is occupied by n_i^{-1} electrons with $\sum_i n_i^{-1} = 2N$ the total number of π-electrons. Particularly, we obtain that $n_i = 1$ when $|i\rangle = |k,\downarrow\rangle$ for $(-\frac{\pi}{2} \leqslant k \leqslant \frac{\pi}{2})$, denoted by the blue solid squares, or $|i\rangle = |k,\uparrow\rangle$ for $(-\frac{\pi}{6} \leqslant k \leqslant \frac{\pi}{3})$, denoted by the red solid circles; $n_i = 2$ when $|i\rangle = |\pm\frac{2\pi}{3},\downarrow\rangle$, denoted by the green squares.

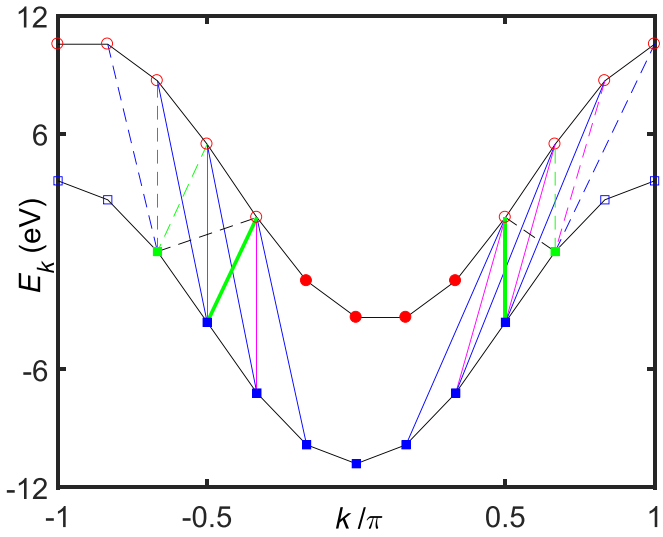

Figure 2. Selection rules for transitions in a Möbius molecule. The curve marked with circles (squares) represents the upper (lower) energy band. The solid red circles and blue squares are the levels occupied by two π electrons with spin up and down, while the empty symbols are unoccupied. The green squares are occupied by one π electron. The curves connecting two bands indicate the selection rules for transitions. Hereafter, we choose the following parameters: $\gamma^{-1} = 4$ ns [30], $V = \xi = 3.6$ eV [63], $W = 0.077$ nm [42], and $R = NW/\pi$.

4. Broad-band negative refraction

According to the selection rules, there are four possible transitions from a given initial state. In order to investigate the effects of simultaneous multi-electron transitions on the negative refraction, we explore the relative permittivity and permeability for different detunings $\Delta\omega = \omega - \Delta_{fi}$. In (21), the lower-band $E_{k,\downarrow}$ is symmetric with respect to $k = 0$, while the upper-band $E_{k,\uparrow}$ is symmetric with respect to $k = \delta/2$. In Figure 2, the following four pairs of transitions possess the same transition frequencies, respectively: $|k, \downarrow\rangle \leftrightarrows |k, \uparrow\rangle$ and $|-k, \downarrow\rangle \leftrightarrows |-k+\delta, \uparrow\rangle$, denoted by the green curves; $|k, \downarrow\rangle \leftrightarrows |k+\delta, \uparrow\rangle$ and $|-k, \downarrow\rangle \leftrightarrows |-k, \uparrow\rangle$, denoted by the magenta curves; $|k, \downarrow\rangle \leftrightarrows |k-\delta, \uparrow\rangle$ and $|-k, \downarrow\rangle \leftrightarrows |-k+2\delta, \uparrow\rangle$, denoted by the black curves; $|k, \downarrow\rangle \leftrightarrows |k+2\delta, \uparrow\rangle$ and $|-k, \downarrow\rangle \leftrightarrows |-k-\delta, \uparrow\rangle$, denoted by the blue curves, which also fulfill the selection rules (3) for the transitions in Möbius molecules.

Generally speaking, the permittivity is a second-rank tensor with nine matrix elements, i.e.

$$\overleftrightarrow{\varepsilon}_r = \sum_{i,j=x,y,z} \varepsilon_r^{i,j} \hat{e}_i \hat{e}_j. \tag{25}$$

In addition to the selection rules of optical transitions, the electric response can only occur at those transitions from the HOMOs to the LUMOs. The relative permittivity $\overleftrightarrow{\varepsilon}_r$ can be further simplified as

$$\overleftrightarrow{\varepsilon}_r = 1 + \sum_{k\in\mathrm{HOMO}} \sum_{k'\in\mathrm{LUMO}} \overleftrightarrow{\chi}^{\mathrm{E}}_{k,k'}, \tag{26}$$

where the components of the tensor

$$\overleftrightarrow{\chi}^{\mathrm{E}}_{k,k'} = \sum_{i,j=x,y,z} \chi^{\mathrm{E},i,j}_{k,k'} \hat{e}_i \hat{e}_j \tag{27}$$

are, respectively,

$$\begin{aligned}
\chi^{\mathrm{E},xx}_{k,k'} &= \chi^{\mathrm{E},yy}_{k,k'} = -\eta'_{k,k'},\\
\chi^{\mathrm{E},zz}_{k,k'} &= -4\eta'_{k,k'},\\
\chi^{\mathrm{E},xy}_{k,k'} &= -\chi^{\mathrm{E},yx}_{k,k'}\\
&= i\eta'_{k,k'}(\delta_{k',k} - \delta_{k',k+\delta} - \delta_{k',k+2\delta} + \delta_{k',k-\delta}),\\
\chi^{\mathrm{E},xz}_{k,k'} &= -\chi^{\mathrm{E},zx}_{k,k'} = i2\eta'_{k,k'}(\delta_{k',k} - \delta_{k',k+\delta}),\\
\chi^{\mathrm{E},yz}_{k,k'} &= \chi^{\mathrm{E},zy}_{k,k'} = -2\eta'_{k,k'}(\delta_{k',k+\delta} + \delta_{k',k}).
\end{aligned}$$

Here, $\eta'_{k,k'}$ is the real part of

$$\eta_{k,k'} = \frac{1}{16\varepsilon_0 v_0}\frac{e^2W^2}{\hbar\omega - (E_{k'\uparrow} - E_{k\downarrow}) + i\hbar\gamma}. \tag{28}$$

Following the same procedure, we can calculate the nine components of the relative permeability, i.e.

$$\overleftrightarrow{\mu}_r = \sum_{i,j=x,y,z} \mu_r^{i,j}\hat{e}_i\hat{e}_j. \tag{29}$$

In addition to the selection rules of optical transitions, the magnetic response can only occur at those transitions from the HOMOs to the LUMOs. The relative permittivity $\overleftrightarrow{\mu}_r$ is related to $\overleftrightarrow{\chi}^{\mathrm{B}}_{k,k'}$ by

$$\overleftrightarrow{\mu}_r = 1 + \sum_{k\in\mathrm{HOMO}}\sum_{k'\in\mathrm{LUMO}} \overleftrightarrow{\chi}^{\mathrm{B}}_{k,k'}, \tag{30}$$

where the components of the tensor

$$\overleftrightarrow{\chi}^{\mathrm{B}}_{k,k'} = \sum_{i,j=x,y,z} \chi^{\mathrm{B},i,j}_{k,k'}\hat{e}_i\hat{e}_j, \tag{31}$$

are, respectively,

$$\begin{aligned}
\chi^{\mathrm{B},xx}_{k,k'} &= \chi^{\mathrm{B},yy}_{k,k'} = -\alpha^2_{k,k'}\eta'_{k,k'},\\
\chi^{\mathrm{B},zz}_{k,k'} &= -4\beta^2_{k,k'}\eta'_{k,k'}(\delta_{k',k+\delta} + \delta_{k',k}),\\
\chi^{\mathrm{B},xy}_{k,k'} &= -\chi^{\mathrm{B},yx}_{k,k'}\\
&= i\alpha^2_{k,k'}\eta'_{k,k'}(\delta_{k',k} - \delta_{k',k+\delta} - \delta_{k',k+2\delta} + \delta_{k',k-\delta}),\\
\chi^{\mathrm{B},xz}_{k,k'} &= -\chi^{\mathrm{B},zx}_{k,k'} = 2i\alpha_{k,k'}\beta_{k,k'}\eta'_{k,k'}(\delta_{k',k} - \delta_{k',k+\delta}),\\
\chi^{\mathrm{B},yz}_{k,k'} &= \chi^{\mathrm{B},zy}_{k,k'} = -2\alpha_{k,k'}\beta_{k,k'}\eta'_{k,k'}(\delta_{k',k+\delta} + \delta_{k',k}).
\end{aligned}$$

with

$$\begin{aligned}
\alpha_{k,k} &= \frac{R}{\hbar c}\left\{V + \varepsilon\left[\cos(k-\delta) - \cos\left(k + \frac{\delta}{2}\right)\right]\right\},\\
\alpha_{k,k+\delta} &= \frac{R}{\hbar c}\left\{V + \varepsilon\left[\cos(k+\delta) - \cos\left(k - \frac{\delta}{2}\right)\right]\right\},\\
\alpha_{k,k+2\delta} &= \frac{R}{\hbar c}\left\{V + \varepsilon\left[\cos(k+\delta) - \cos\left(k + \frac{\delta}{2}\right)\right]\right\},\\
\alpha_{k,k-\delta} &= \frac{R}{\hbar c}\left\{V + \varepsilon\left[\cos(k-\delta) - \cos\left(k - \frac{\delta}{2}\right)\right]\right\},\\
\beta_{k,k} &= -\frac{2R\varepsilon}{\hbar c}\sin\left(k - \frac{\delta}{4}\right)\sin\delta\cos\frac{\delta}{4},\\
\beta_{k,k+\delta} &= \frac{2R\varepsilon}{\hbar c}\sin\left(k + \frac{\delta}{4}\right)\sin\delta\cos\frac{\delta}{4}.
\end{aligned}$$

In figure 3, we show the widest bandwidth for the negative refraction which corresponds to the transitions labeled by the thick green curves in figure 2. The bandwidth of the negative refraction is 80 μeV, which is about 20 *times* that of [30]. To explore the underlying broadening mechanism, we investigate the relevant contributions from all simultaneous transitions. Generally, the magnetic response is much smaller than the electric response. In appendix B, it was proven that for *E*-polarized incident fields, the bandwidth is determined by the zeros of smallest principal value of the negative permeability. Therefore, the bandwidth of the negative refraction is mainly given by bandwidth of the negative permeability. In figure 4, we investigate the effect of simultaneous transitions on the negative refraction by the relative permeability. At the transition frequency, there are two degenerate transitions, denoted by the thick green curves in figure 2. One is from the initial state $\left|-\frac{\pi}{2}, \downarrow\right\rangle$ to the final state $\left|-\frac{\pi}{3}, \uparrow\right\rangle$, denoted by the green circles in figure 4. The other transition is from $\left|\frac{\pi}{2}, \downarrow\right\rangle$ to $\left|\frac{\pi}{2}, \uparrow\right\rangle$, denoted by the black curve. The summation of the two transitions, denoted by the red dotted curve, is nearly the same as that of all contributions.

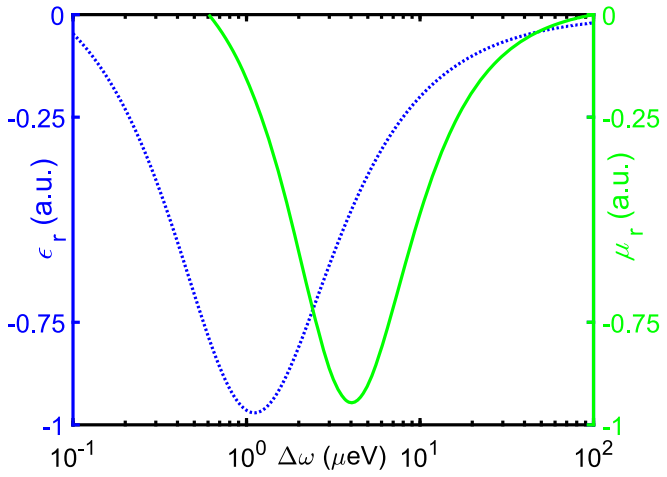

Figure 3. Relative permittivity ε_r (blue dotted curve) and permeability μ_r (green curve) of Möbius molecules versus the detuning $\Delta\omega$. Here we only show the lowest eigenvalue.

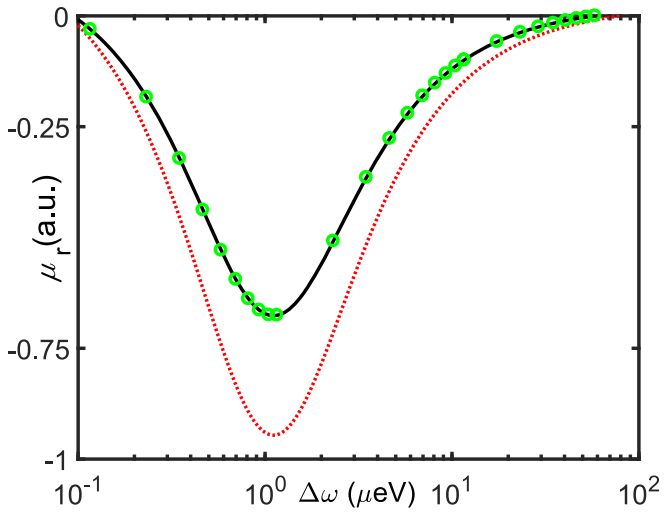

Figure 4. Effects of simultaneous multi-electron transitions and enhanced transition dipole on the relative permeability of Möbius molecules. The green circles is for $\left|-\frac{\pi}{2}, \downarrow\right\rangle \rightleftarrows \left|-\frac{\pi}{3}, \uparrow\right\rangle$, and the black curve are for $\left|\frac{\pi}{2}, \downarrow\right\rangle \rightleftarrows \left|\frac{\pi}{2}, \uparrow\right\rangle$, and the red dotted curve sums up the two resonant transitions.

For the transitions $|k, \downarrow\rangle \leftrightarrows |k', \uparrow\rangle$ ($k' = k,\ k+\delta$), the three eigenvalues of $\overleftrightarrow{\mu}_r$ are, respectively,

$$\mu_r^1 = 1 - 2\sum_{k,k'} \alpha_{k,k'}^2 \eta'_{k,k'},$$

$$\mu_r^2 = 1 - 2\sum_{k,k'} (\beta_{k,k'}^2 + \beta_{k,k'}\sqrt{2\alpha_{k,k'}^2 + \beta_{k,k'}^2})\eta'_{k,k'},$$

$$\mu_r^3 = 1 - 2\sum_{k,k'} (\beta_{k,k'}^2 - \beta_{k,k'}\sqrt{2\alpha_{k,k'}^2 + \beta_{k,k'}^2})\eta'_{k,k'}.$$

For the transitions $|k, \downarrow\rangle \leftrightarrows |k', \uparrow\rangle$ ($k' = k-\delta,\ k+2\delta$), the three eigenvalues of $\overleftrightarrow{\mu}_r$ are, respectively,

$$\mu_r^1 = 1 - 2\sum_{k,k'} \alpha_{k,k'}^2 \eta'_{k,k'},\ \ \mu_r^2 = \mu_r^3 = 1.$$

In both cases, the lowest eigenvalue is μ_r^1, because $(\beta_{k,k'}/\alpha_{k,k'})^2 \sim \delta^2 \ll 1$. The bandwidth of the negative refraction is determined by the zeros of the lowest eigenvalue of $\overleftrightarrow{\mu}_r$, i.e.

$$\mu_r^1 = 1 - \sum_{k,k'} 2\alpha_{k,k'}^2 \eta'_{k,k'} = 0, \tag{32}$$

Table 1. Comparison of the bandwidths (BWs) of the negative refraction in the literatures and present paper.

References	Present	[30]	[23, 24]	[36]	[34]
BW (Hz)	1.9×10^{10}	0.97×10^{9}	2×10^{5}	5.0×10^{4}	1.6×10^{8}

Table 2. The bandwidths (BWs) of the negative refraction around different transition frequencies Δ_{if}. In the third column, the participating transitions are explicitly given.

BW (μeV)	participating transitions
80	$\lvert\frac{\pi}{2}, \downarrow\rangle \rightleftarrows \lvert\frac{\pi}{2}, \uparrow\rangle, \lvert-\frac{\pi}{2}, \downarrow\rangle \rightleftarrows \lvert-\frac{\pi}{3}, \uparrow\rangle$
36	$\lvert\frac{2\pi}{3}, \downarrow\rangle \rightleftarrows \lvert\frac{2\pi}{3}, \uparrow\rangle, \lvert-\frac{2\pi}{3}, \downarrow\rangle \rightleftarrows \lvert-\frac{\pi}{2}, \uparrow\rangle$
15	$\lvert\frac{2\pi}{3}, \downarrow\rangle \rightleftarrows \lvert\frac{5\pi}{6}, \uparrow\rangle, \lvert-\frac{2\pi}{3}, \downarrow\rangle \rightleftarrows \lvert-\frac{2\pi}{3}, \uparrow\rangle$
39	$\lvert\frac{\pi}{3}, \downarrow\rangle \rightleftarrows \lvert\frac{\pi}{2}, \uparrow\rangle, \lvert-\frac{\pi}{3}, \downarrow\rangle \rightleftarrows \lvert-\frac{\pi}{3}, \uparrow\rangle$
45	$\lvert\frac{\pi}{2}, \downarrow\rangle \rightleftarrows \lvert\frac{2\pi}{3}, \uparrow\rangle, \lvert-\frac{\pi}{2}, \downarrow\rangle \rightleftarrows \lvert-\frac{\pi}{2}, \uparrow\rangle$

where $\eta'_{k,k'}$ is of the same form for different transitions but with a different central frequency. Among four possible $\alpha_{k,k'}$'s, the maximum of $\alpha_{k,k}$ and $\alpha_{k,k+\delta}$ are generally larger than those of $\alpha_{k,k-\delta}$ and $\alpha_{k,k+2\delta}$. Assuming that $\varepsilon = V$, we have

$$\alpha_{\frac{\pi}{2},\frac{\pi}{2}} \simeq \frac{RV}{\hbar c}\left(1 + 2\sin\frac{3\delta}{4}\right) \simeq \frac{7RV}{4\hbar c}, \tag{33}$$

$$\alpha_{-\frac{\pi}{2},-\frac{\pi}{3}} \simeq \frac{RV}{\hbar c}\left(1 + 2\sin\frac{3\delta}{4}\right) \simeq \frac{7RV}{4\hbar c}. \tag{34}$$

In [30], negative refraction was considered for the single transition $\lvert 0, \downarrow\rangle \rightleftarrows \lvert 0, \uparrow\rangle$ with

$$\alpha_{0,0} \simeq \frac{RV}{\hbar c}\left(1 - 2\sin\frac{\delta}{2}\sin\frac{3\delta}{4}\right) \simeq \frac{13RV}{16\hbar c}. \tag{35}$$

Since $\alpha^2_{\frac{\pi}{2},\frac{\pi}{2}} = \alpha^2_{-\frac{\pi}{2},-\frac{\pi}{3}} \simeq 5\alpha^2_{0,0}$,the transition dipoles have been enlarged by a factor of $\sqrt{5}$. Furthermore,there are four simultaneous transitions with the same transition frequency,i.e. $\left|\frac{\pi}{2}, \downarrow\right\rangle \rightleftarrows \left|\frac{\pi}{2}, \uparrow\right\rangle$ and $\left|-\frac{\pi}{2}, \downarrow\right\rangle \rightleftarrows \left|-\frac{\pi}{3}, \uparrow\right\rangle$ with two different electronic spins,the bandwidth of the negative refraction is about 20 times of our previous observation in [30]. Compared to other discoveries as listed in table 1,our proposed bandwidth is about: 10^5 *times* that of [23, 24],4×10^5 *times* that of [36],and 121 *times* that of [34].

As shown in figure 2, there are 20 possible transitions on account of the initial condition, where there is an electron occupying the HOMOs, and the final condition, where there is no electron occupying the LUMOs. By scanning over all transition frequencies, we obtain the bandwidths of the negative refraction for all transitions, as listed in table 2. Due to simultaneous multi-electron transitions, the bandwidths of the negative refraction are generally larger than the corresponding single-electron transition and that in [30]. Interestingly, the bandwidths of five transitions are larger than the previous observation by one order of magnitude.

5. Discussion and conclusions

In the previous sections, we use the Möbius molecule as an example to demonstrate broad-band metamaterials by simultaneous multi-electron transitions. Although the currently broadened bandwidth, 22.2 GHz, is much narrower than that of the traditional split-ring resonator, 10 THz [64], we show that this scheme might be possibly applied to other solids. In [22], due to anisotropic electric response to the applied electromagnetic fields, the diamond with NV centers can realize hyperbolic dispersion relation and thus negative refraction with bandwidth about 10GHz at the room temperature. The experimental observation of the NV center suggested a six-electron model [65, 66], where the electrons consist of the five unpaired electrons of the nearest-neighbour nitrogen and carbon atoms to the vacancy and an additional trapped electron. The manifold of the electronic ground state includes spin-triplet states, i.e. $\lvert\Phi^c_{A_2;1,m_s}\rangle$ $(m_s = \pm 1, 0)$ with $\lvert\Phi^c_{A_2;1,\pm 1}\rangle$ degenerate in the absence of static magnetic fields. The manifold of the electronic excited state contains two sets of spin-triplet states, i.e. $\lvert\Phi^c_{E,x;1,m_s}\rangle$ and $\lvert\Phi^c_{E,y;1,m_s}\rangle$. When the static magnetic fields and strain fields are absent, there are two sets of two transitions with the same transition frequencies, respectively. Notice that the bandwidth is inversely proportional to the square decoherence rates of excited states, cf equations (10), (11). The bandwidth can be increased by nearly 2 orders of magnitude if the temperature is decreased to 10 K due to a sharp decline of the

decoherence rate from 0.1 GHz to 16.2 MHz [67]. If the density of NV centers is further increased to 10 ppm, a bandwidth of negative refraction about 45.4 THz may be observed.

To summarize, we explore the possibility of significantly broadening the negative refraction of metamaterials by simultaneous multi-electron transitions. As a specific example, we calculate the optical properties of Möbius molecules based on the Hückel molecular orbital method and linear-response theory. The simultaneous multi-electron transitions provide parallel contributions to the overlapping negative refraction. Furthermore, in each transition, the negative refraction is significantly broadened by the enhanced transition dipole. As a result of these two broadening effects, the bandwidth for the negative refraction is larger than the previous discoveries in [23, 34] by at least *two* orders of magnitude. Therefore, we clearly show that the contributions of multi-electron transitions and enhanced transition dipoles can lead to a large broadening of the negative-index interval. Moreover, as metamaterials consisting of Möbius molecules are based on quantum transitions, their size is smaller by 2 orders of magnitude than in classical metamaterials. Instead of producing a huge number of split-ring resonators, metamaterials of Möbius molecules are chemically synthesized and self-assembled by crystallization. In conclusion, this work provides a possible route for broad-band negative refractive-index of metamaterials.

Acknowledgments

We thank stimulating discussions with Y N Fang and T Tanaka. This work was supported by the National Natural Science Foundation of China under Grant Nos. 11505007 and 11474026, MURI Center for Dynamic Magneto-Optics via the Air Force Office of Scientific Research (AFOSR) (FA9550-14-1-0040), Army Research Office (ARO) (Grant No. W911NF-18-1-0358), Asian Office of Aerospace Research and Development (AOARD) (Grant No. FA2386-18-1-4045), Japan Science and Technology Agency (JST) (via the Q-LEAP program, the ImPACT program, and the CREST Grant No. JPMJCR1676), Japan Society for the Promotion of Science (JSPS) (JSPS-RFBR Grant No. 17-52-50023, and JSPS-FWO Grant No. VS.059.18N), the RIKEN-AIST Challenge Research Fund, and the John Templeton Foundation.

Appendix A. Transition matrices of electric and magnetic dipoles

In section 2, we apply linear-response theory to rewrite the relative permittivity and permeability in terms of the transition matrix elements of the electric and magnetic dipole, i.e. $\vec{d}_{if}$ and $\vec{m}_{if}$. According to (10), (11), we would expect the negative permittivity and permeability to be close to the transition frequency Δ_{fi}. Hereafter, the selection rules of transitions are explicitly provided by calculating the matrix elements of the electric and magnetic dipole.

Under the dipole approximation, the interaction Hamiltonian with the electric field is written as [31, 32]

$$H'_E = -\vec{d}\cdot\vec{E}_0\cos\omega t. \tag{A.1}$$

The electric-dipole-induced transition is allowed if the corresponding matrix element is nonzero. By using the relation $\langle\phi_{js}|\ \vec{r}|\phi_{j's'}\rangle = \vec{R}_{js}\delta_{jj'}\delta_{ss'}$ [59], the non-vanishing matrix elements are explicitly listed as

$$\begin{aligned}
\langle 0|\ C_{k\uparrow}H'_E C^{\dagger}_{k\downarrow}|0\rangle &= \left(i\frac{E_0^x}{4}+\frac{E_0^y}{4}+\frac{E_0^z}{2}\right)eW\cos\omega t,\\
\langle 0|\ C_{k\uparrow}H'_E C^{\dagger}_{k+\delta,\uparrow}|0\rangle &= \left(\frac{E_0^x}{2}-i\frac{E_0^y}{2}\right)eR\cos\omega t,\\
\langle 0|\ C_{k\uparrow}H'_E C^{\dagger}_{k+\delta,\downarrow}|0\rangle &= \left(-i\frac{E_0^x}{4}-\frac{E_0^y}{4}\right)eW\cos\omega t,\\
\langle 0|\ C_{k\downarrow}H'_E C^{\dagger}_{k+\delta,\uparrow}|0\rangle &= \left(i\frac{E_0^x}{4}+\frac{E_0^y}{4}+\frac{E_0^z}{2}\right)eW\cos\omega t,\\
\langle 0|\ C_{k\downarrow}H'_E C^{\dagger}_{k+\delta,\downarrow}|0\rangle &= \left(\frac{E_0^x}{2}-i\frac{E_0^y}{2}\right)eR\cos\omega t,\\
\langle 0|\ C_{k\uparrow}H'_E C^{\dagger}_{k-\delta,\uparrow}|0\rangle &= \left(\frac{E_0^x}{2}+i\frac{E_0^y}{2}\right)eR\cos\omega t,\\
\langle 0|\ C_{k\downarrow}H'_E C^{\dagger}_{k-\delta,\downarrow}|0\rangle &= \left(\frac{E_0^x}{2}+i\frac{E_0^y}{2}\right)eR\cos\omega t,\\
\langle 0|\ C_{k\downarrow}H'_E C^{\dagger}_{k+2\delta,\uparrow}|0\rangle &= \left(-i\frac{E_0^x}{4}-\frac{E_0^y}{4}\right)eW\cos\omega t.
\end{aligned} \tag{A.2}$$

For example, because in the above equations, the matrix element is nonzero between the states $|k,\uparrow\rangle\rangle$ and $|k,\downarrow\rangle\rangle$, and there are contributions from all three components of the electric field, the transition $|k,\uparrow\rangle\rangle \rightleftharpoons |k,\downarrow\rangle\rangle$ can be electric-dipole induced for all three polarizations of the electric field. Based on the above equations, the selection rules for the electric-dipole-induced transitions are summarized as (3).

Under the dipole approximation, the interaction Hamiltonian with the magnetic field is written as [31, 32]

$$H'_B = -\vec{m}\cdot\vec{B}_0\cos\omega t. \tag{A.3}$$

Straightforward calculations show the following non-vanishing matrix elements,

$$\begin{aligned}
\langle 0|\ C_{k\uparrow}H'_B C^{\dagger}_{k\uparrow}|0\rangle &= -\{2W^2[\cos(k-\delta)-\cos k]B_0^y + [W^2(\cos k-\cos(k-2\delta)\\
&\quad -\cos(k-\delta)+\cos(k+\delta)) + 4R^2\left(\cos\left(k+\frac{\delta}{2}\right)-\cos\left(k-\frac{3}{2}\delta\right)\right)\Big]B_0^z\Big\}\frac{e\xi}{8\hbar}\cos\omega t,\\
\langle 0|\ C_{k\uparrow}H'_B C^{\dagger}_{k\downarrow}|0\rangle &= -\Big\{\Big[V+\xi\left(\cos(k-\delta)-\cos\left(k+\frac{\delta}{2}\right)\right)\Big](B_0^x - iB_0^y)\\
&\quad + 2i\xi\cos\frac{\delta}{4}\left[\cos\left(k-\frac{5\delta}{4}\right)-\cos\left(k+\frac{3}{4}\delta\right)\right]B_0^z\Big\}\frac{eRW}{4\hbar}\cos\omega t,\\
\langle 0|\ C_{k\downarrow}H'_B C^{\dagger}_{k\downarrow}|0\rangle &= -\left[W^2B_0^y\sin\frac{\delta}{2}-\left(2R^2+W^2\cos\frac{\delta}{2}\right)B_0^z\sin\delta\right]\frac{e\xi}{2\hbar}\sin k\cos\omega t,\\
\langle 0|\ C_{k\uparrow}H'_B C^{\dagger}_{k+\delta,\uparrow}|0\rangle &= [\cos(k-\delta)-\cos(k+\delta)](iB_0^x+B_0^y-B_0^z)\frac{eW^2\xi}{8\hbar}\cos\omega t,\\
\langle 0|\ C_{k\uparrow}H'_B C^{\dagger}_{k+\delta,\downarrow}|0\rangle &= -\Big\{\Big[V+\xi\left(\cos k-\cos\left(k+\frac{\delta}{2}\right)\right)\Big](B_0^x-iB_0^y)\\
&\quad -2i\xi\cos\frac{\delta}{4}\left[\cos\left(k-\frac{5\delta}{4}\right)-\cos\left(k+\frac{3}{4}\delta\right)\right]B_0^z\Big\}\frac{eRW}{8\hbar}\cos\omega t,\\
\langle 0|\ C_{k\downarrow}H'_B C^{\dagger}_{k+\delta,\uparrow}|0\rangle &= \Big\{\Big[V+\xi\left(\cos(k+\delta)-\cos\left(k-\frac{\delta}{2}\right)\right)\Big](B_0^x-iB_0^y) - i\xi[\cos(k-\delta)\\
&\quad -\cos(k+\delta)-\cos\left(k+\frac{3\delta}{2}\right)+\cos\left(k-\frac{\delta}{2}\right)\Big]B_0^z\Big\}\frac{eRW}{4\hbar}\cos\omega t,\\
\langle 0|\ C_{k\downarrow}H'_B C^{\dagger}_{k+\delta,\downarrow}|0\rangle &= \left[\cos\left(k-\frac{\delta}{2}\right)-\cos\left(k+\frac{3\delta}{2}\right)\right](iB_0^x+B_0^y-B_0^z)\frac{eW^2\xi}{8\hbar}\cos\omega t,\\
\langle 0|\ C_{k\uparrow}H'_B C^{\dagger}_{k-\delta,\uparrow}|0\rangle &= -[\cos(k-2\delta)-\cos k](iB_0^x-B_0^y+B_0^z)\frac{eW^2\xi}{8\hbar}\cos\omega t,\\
\langle 0|\ C^{\dagger}_{k\downarrow}H'_B C_{k-\delta,\uparrow}|0\rangle &= -\left\{V+\xi\left[\cos(k-\delta)-\cos\left(k-\frac{\delta}{2}\right)\right]\right\}(B_0^x+iB_0^y)\frac{eRW}{4\hbar}\cos\omega t,\\
\langle 0|\ C_{k\downarrow}H'_B C^{\dagger}_{k-\delta,\downarrow}|0\rangle &= \left[\cos\left(k-\frac{3\delta}{2}\right)-\cos\left(k+\frac{\delta}{2}\right)\right](-iB_0^x+B_0^y-B_0^z)\frac{eW^2\xi}{8\hbar}\cos\omega t,\\
\langle 0|\ C_{k\uparrow}H'_B C^{\dagger}_{k+2\delta,\uparrow}|0\rangle &= i[\cos k-\cos(k+\delta)](B_0^x-iB_0^y)\frac{eW^2\xi}{8\hbar}\cos\omega t,\\
\langle 0|\ C_{k\downarrow}H'_B C^{\dagger}_{k+2\delta,\uparrow}|0\rangle &= \left\{V+\xi\left[\cos(k+\delta)-\cos\left(k+\frac{\delta}{2}\right)\right]\right\}(B_0^x-iB_0^y)\frac{eRW}{4\hbar}\cos\omega t,\\
\langle 0|\ C_{k\downarrow}H'_B C^{\dagger}_{k+2\delta,\downarrow}|0\rangle &= i\left[\cos\left(k+\frac{\delta}{2}\right)-\cos\left(k+\frac{3\delta}{2}\right)\right](B_0^x-iB_0^y)\frac{eW^2\xi}{8\hbar}\cos\omega t.
\end{aligned} \tag{A.4}$$

Therefore, we have the same selection rules for the magnetic-dipole-induced transitions as given in (3).

Appendix B. *E*-polarized incident fields

For the transitions $|k,\downarrow\rangle \leftrightarrows |k',\uparrow\rangle$ ($k' = k,\ k+\delta$), the relative permittivity is approximated as

$$\overleftrightarrow{\varepsilon}_r = \begin{bmatrix} 1-4\eta'_{kk} & 0 & 0\\ 0 & 1-4\eta'_{kk} & -8\eta'_{kk}\\ 0 & -8\eta'_{kk} & 1-16\eta'_{kk}\end{bmatrix}. \tag{B.1}$$

Generally, $\beta_{kk'}$ is smaller than $\alpha_{kk'}$ by one order of magnitude. To the zeroth order of $\beta_{kk'}$, the relative permeability is approximated as

$$\overleftrightarrow{\mu}_r = \begin{bmatrix} 1 - 4\alpha_{kk}^2\eta'_{kk} & 0 & 0 \\ 0 & 1 - 4\alpha_{kk}^2\eta'_{kk} & 0 \\ 0 & 0 & 1 \end{bmatrix}. \tag{B.2}$$

When an E-polarized electromagnetic field,

$$\vec{E}_i = E_0\hat{e}_x e^{i(k_{iy}y + k_{iz}z - \omega t)}, \tag{B.3}$$

is incident on the metamaterial, the refracted field,

$$\vec{E}_t = t_c E_0\hat{e}_x e^{i(k_{iy}y + k_{tz}z - \omega t)}, \tag{B.4}$$

is governed by the Helmholtz equation

$$\vec{k}_t \times [(\overleftrightarrow{\mu}_r)^{-1}(\vec{k}_t \times \vec{E}_t)] = -\omega^2\mu_0\varepsilon_0\overleftrightarrow{\varepsilon}_r\vec{E}_t. \tag{B.5}$$

By inserting (B.1), (B.2) into the above equation, we obtain

$$\varepsilon_r^{(xx)}k_i^2 - k_{ty}^2 - (\mu_r^{(yy)})^{-1}k_{tz}^2 = 0, \tag{B.6}$$

with the solution

$$k_{tz} = k_i\sqrt{(1 - 4\alpha_{kk}^2\eta'_{kk})(\cos^2\theta - 4\eta'_{kk})}. \tag{B.7}$$

The refracted magnetic field can be calculated by the Maxwell equation $\vec{k}_t \times \vec{E}_t = \omega\mu_0\overleftrightarrow{\mu}_r\vec{H}_t$ as

$$H_t = \frac{t_c E_x}{\omega\mu_0}(-k_{ty}\hat{e}_z + \frac{k_{tz}}{\mu_r^{yy}}\hat{e}_y). \tag{B.8}$$

Therefore, the time-averaged Poynting vector vector of the refracted electromagnetic field is

$$\vec{S}_t = \frac{1}{2}\mathrm{Re}\,(\vec{E}_t \times \vec{H}_t^*) = \frac{t_c^2E_x^2}{2\omega\mu_0}\left(k_{ty}\hat{e}_y + \frac{k_{tz}}{\mu_r^{yy}}\hat{e}_z\right). \tag{B.9}$$

The occurrence of negative refraction is determined by the following three criteria, i.e.

$$0 > \vec{k}_t \cdot \vec{S}_t, \tag{B.10}$$

$$0 < (1 - 4\alpha_{kk}^2\eta'_{kk})(\cos^2\theta - 4\eta'_{kk}), \tag{B.11}$$

$$0 < S_{tz} = \frac{k_{tz}t_c^2E_x^2}{2\omega\mu_0(1 - 4\alpha_{kk}^2\eta'_{kk})}, \tag{B.12}$$

where the first criterion implies the reversal of the phase velocity to the Poynting vector, the second criterion requires a real wavevector in the metamaterial, the last criterion is required by the causality that the normal component of its Poynting vector is in the same direction as that for the incident light. The bandwidth of negative refraction is determined by the zeros of the second equation, i.e. $(1 - 4\alpha_{kk}^2\eta'_{kk})(\cos^2\theta - 4\eta'_{kk}) = 0$, which is confirmed by our numerical simulation. Since $\alpha_{kk}^2 \ll 1$, the bandwidth is given by the zeros of $1 - 4\alpha_{kk}^2\eta'_{kk} = 0$, which is consistent with our analysis presented in the main text.

ORCID iDs

Qing Ai https://orcid.org/0000-0002-0116-7844

References

[1] Veselago V G 1968 The electrodynamics of substances with simultaneously negative values of ε and μ *Sov. Phys. Uspekhi* **10** 509–14
[2] Pendry J B 2000 Negative refraction makes a perfect lens *Phys. Rev. Lett.* **85** 3966–9
[3] Smith D R, Padilla W J, Vier D C, Nemat-Nasser S C and Schultz S 2000 Composite medium with simultaneously negative permeability and permittivity *Phys. Rev. Lett.* **84** 4184–7
[4] Bliokh K Y, Bliokh Y P, Freilikher V, Savel'ev S and Nori F 2008 Colloquium: unusual resonators: plasmonics, metamaterials, and random media *Rev. Mod. Phys.* **80** 1201–13
[5] Khorasaninejad M and Capasso F 2017 Metalenses: versatile multifunctional photonic components *Science* **358** 1146–53
[6] Minovich A E, Miroshnichenko A E, Bykov A Y, Murzina T V, Neshev D N and Kivshar Y S 2015 Functional and nonlinear optical metasurfaces *Laser Photonics Rev.* **9** 195–213
[7] Zhao R K, Luo Y and Pendry J B 2016 Transformation optics applied to van der Waals interactions *Sci. Bull.* **61** 59–67
[8] Lee H, Xiong Y, Fang N, Srituravanich W, Durant S, Ambati M, Sun C and Zhang X 2005 Realization of optical superlens imaging below the diffraction limit *New J. Phys.* **7** 255

[9] Shen Y and Ai Q 2016 Optical properties of drug metabolites in latent fingermarks *Sci. Rep.* **6** 20336
[10] Bliokh Y P, Freilikher V and Nori F 2013 Ballistic charge transport in graphene and light propagation in periodic dielectric structures with metamaterials: a comparative study *Phys. Rev.* B **87** 245134
[11] Kats A V, Savel'ev S, Yampol'skii V A and Nori F 2007 Left-handed interfaces for electromagnetic surface waves *Phys. Rev. Lett.* **98** 073901
[12] Jiang S C, Xiong X, Hu Y S, Hu Y H, Ma G B, Peng R W, Sun C and Wang M 2014 Controlling the polarization state of light with a dispersion-free metastructure *Phys. Rev.* X **4** 021026
[13] Leonhardt U 2006 Optical conformal mapping *Science* **312** 1777–80
[14] Pendry J B, Schurig D and Smith D R 2006 Controlling electromagnetic fields *Science* **312** 1780–2
[15] Rainwater D, Kerkhoff A, Melin K, Soric J C, Moreno G and Alu A 2012 Experimental verification of three-dimensional plasmonic cloaking in free-space *New J. Phys.* **14** 013054
[16] Xiong X, Jiang S C, Hu Y H, Peng R W and Wang M 2013 Structured metal film as a perfect absorber *Adv. Mater.* **25** 3994–4000
[17] Shen Y, Ko H Y, Ai Q, Peng S M and Jin B Y 2014 Molecular split-ring resonators based on metal string complexes *J. Phys. Chem.* C **118** 3776
[18] Pendry J B 2004 A chiral route to negative refraction *Science* **306** 1353–5
[19] Fisher R K and Gould R W 1969 Resonance cones in the field pattern of a short antenna in an anisotropic plasma *Phys. Rev. Lett.* **22** 1093–5
[20] Smith D R and Schurig D 2003 Electromagnetic wave propagation in media with indefinite permittivity and permeability tensors *Phys. Rev. Lett.* **90** 077405
[21] Rakhmanov A L, Yampol'skii V A, Fan J A, Capasso F and Nori F 2010 Layered superconductors as negative-refractive-index metamaterials *Phys. Rev.* B **81** 075101
[22] Ai Q, Li P B, Qin W, Sun C P and Nori F 2018 NV-Metamaterial: tunable quantum hyperbolic metamaterial using nitrogen-vacancy centers in diamond arXiv:1802.01280
[23] Kästel J, Fleischhauer M, Yelin S F and Walsworth R L 2007 Tunable negative refraction without absorption via electromagnetically induced chirality *Phys. Rev. Lett.* **99** 073602
[24] Kästel J, Fleischhauer M and Juzeliūnas G 2007 Local-field effects in magnetodielectric media: negative refraction and absorption reduction *Phys. Rev.* A **76** 062509
[25] Kästel J, Fleischhauer M, Yelin S F and Walsworth R L 2009 Low-loss negative refraction by laser-induced magnetoelectric cross coupling *Phys. Rev.* A **79** 063818
[26] Qin L, Zhang K, Peng R W, Xiong X, Zhang W, Huang X R and Wang M 2013 Optical-magnetism-induced transparency in a metamaterial *Phys. Rev.* B **87** 125136
[27] Wang Y Y, Qiu J, Chu Y Q, Zhang M, Cai J M, Ai Q and Deng F G 2018 Dark state polarizing a nuclear spin in the vicinity of a nitrogen-vacancy center *Phys. Rev.* A **97** 042313
[28] Chang C W, Liu M, Nam S, Zhang S, Liu Y, Bartal G and Zhang X 2010 Optical Möbius symmetry in metamaterials *Phys. Rev. Lett.* **105** 235501
[29] Krishnamoorthy H N S, Jacob Z, Narimanov E, Kretzschmar I and Menon V M 2012 Topological transitions in metamaterials *Science* **336** 205–9
[30] Fang Y N, Shen Y, Ai Q and Sun C P 2016 Negative refraction in Möbius molecules *Phys. Rev.* A **94** 043805
[31] Landau L D, Lifshitz E M and Pitaevskii L P 1995 *Electrodynamics of Continuous Media* (Oxford: Butterworth Heinmann)
[32] Jackson J D 1999 *Classical Electrodynamics* (United States: Wiley)
[33] Chen Y F, Fischer P and Wise F W 2005 Negative refraction at optical frequencies in nonmagnetic two-component molecular media *Phys. Rev. Lett.* **95** 067402
[34] Thommen Q and Mandel P 2006 Electromagnetically induced left handedness in optically excited four-level atomic media *Phys. Rev. Lett.* **96** 053601
[35] Orth P P, Hennig R, Keitel C H and Evers J 2013 Negative refraction with tunable absorption in an active dense gas of atoms *New J. Phys.* **15** 013027
[36] Oktel M Ö and Müstecaplıoğlu Ö E 2004 Electromagnetically induced left-handedness in a dense gas of three-level atoms *Phys. Rev.* A **70** 053806
[37] Ceulemans A, Chibotaru L F and Fowler P W 1998 Molecular anapole moments *Phys. Rev. Lett.* **80** 1861–4
[38] Zagoskin A M, Chipouline A, Il'ichev E, Johansson J R and Nori F 2015 Toroidal qubits: naturally-decoupled quiet artificial atoms *Sci. Rep.* **5** 16934
[39] Heilbronner E 1964 Hückel molecular orbitals of Möbius-type conformations of annulenes *Tetrahedron Lett.* **5** 1923–8
[40] Walba D M, Homan T C, Richards R M and Haltiwanger R C 1993 Topological stereochemistry. IX: synthesis and cutting in half of a molecular Möbius strip *New J. Chem.* **17** 661–81
[41] Ajami D, Oeckler O, Simon A and Herges R 2003 Synthesis of a Möbius aromatic hydrocarbon *Nature* **426** 819–21
[42] Yoneda T, Sung Y M, Lim J M, Kim D and Osuka A 2014 The largest Hückel aromatic and antiaromatic, and Möbius aromatic macrocycles *Angew. Chem. Int. Ed.* **126** 13385–13173
[43] Fan Y Y, Chen D D, Huang Z A, Zhu J, Tung C H, Wu L Z and Cong H 2018 An isolable catenane consisting of two Möbius conjugated nanohoops *Nature Commun.* **9** 3037
[44] Poddar A K and Rohde U L 2014 Möbius strips and metamaterial symmetry: theory and applications *Microwave J.* **57** 76–84 http://www.microwavejournal.com/articles/23303-mbius-strips-and-metamaterial-symmetry-theory-and-applications?v=preview
[45] Balzani V, Credi A and Venturi M 2008 *Molecular Devices and Machines. Concepts and Perspectives for the Nanoworld* (Weinheim: VCH-Wiley)
[46] Yamashiroa A, Shimoia Y, Harigayaa K and Wakabayashi K 2004 Novel electronic states in graphene ribbons-competing spin and charge orders *Physica* E **22** 688–91
[47] Zhao N, Dong H, Yang S and Sun C P 2009 Observable topological effects in molecular devices with Möbius topology *Phys. Rev.* B **79** 125440
[48] Pond J M 2000 Möbius dual-mode resonators and bandpass filters *IEEE Trans. Microw. Theory Tech.* **48** 2465–71
[49] Guo Z L, Gong Z R, Dong H and Sun C P 2009 Möbius graphene strip as a topological insulator *Phys. Rev.* B **80** 195310
[50] Lukin O and Vögtle F 2005 Knotting and threading of molecules: chemistry and chirality of molecular knots and their assemblies *Angew. Chem. Int. Ed.* **44** 1456–77
[51] Xu L, Gong Z R, Tao M J and Ai Q 2018 Artificial light harvesting by dimerized Möbius ring *Phys. Rev.* E **97** 042124
[52] Lambert N, Chen Y N, Cheng Y C, Chen G Y and Nori F 2013 Quantum biology *Nature Phys.* **9** 10–8

[53] Kubo R, Toda M and Hashitsume N 1985 *Statistical Physics II Nonequlibirum Statistical Mechanics* (Berlin Heidelberg: Springer)
[54] Olaya-Castro A, Lee C F, Olsen F F and Johnson N F 2008 Efficiency of energy transfer in a light-harvesting system under quantum coherence *Phys. Rev.* B **78** 085115
[55] Ai Q, Fan Y J, Jin B Y and Cheng Y C 2014 An efficient quantum jump method for coherent energy transfer dynamics in photosynthetic systems under the influence of laser field *New J. Phys.* **16** 053033
[56] Jang S J and Mennucc B 2018 Delocalized excitons in natural light harvesting complexes *Rev. Mod. Phys.* **90** 035003
[57] Novoderezhkin V I and van Grondelle R 2010 Physical origins and models of energy transfer in photosynthetic light-harvesting *Phys. Chem. Chem. Phys.* **12** 7352–65
[58] Cheng Y C and Silbey R J 2006 Coherence in the B800 ring of purple bacteria LH2 *Phys. Rev. Lett.* **96** 028103
[59] Salem L 1972 *The Molecular Orbital Theory of Conjugated Systems* (Reading, MA: Benjamin)
[60] Ai Q, Li Y, Zheng H and Sun C P 2010 Quantum anti-Zeno effect without rotating wave approximation *Phys. Rev.* A **81** 042116
[61] Wang X, Miranowicz A, Li H R and Nori F 2017 Observing pure effects of counter-rotating terms without ultrastrong coupling: a single photon can simultaneously excite two qubits *Phys. Rev.* A **96** 063820
[62] Zheng H, Zhu S Y and Zubairy M S 2008 Quantum Zeno and anti-Zeno effects: without the rotating-wave approximation *Phys. Rev. Lett.* **101** 200404
[63] Greenwood H H 1972 *Computing Methods in Quantum Organic Chemistry* (Germany: Wiley-Interscience)
[64] Zhou J, Koschny T, Kafesaki M, Economou E N, Pendry J B and Soukoulis C M 2005 Saturation of the magnetic response of split-ring resonators at optical frequencies *Phys. Rev. Lett.* **95** 223902
[65] Doherty M W, Manson N B, Delaney P and Hollenberg L C L 2011 The negatively charged nitrogen-vacancy centre in diamond: the electronic solution *New J. Phys.* **13** 025019
[66] Maze J R, Gali A, Togan E, Chu Y, Trifonov A, Kaxiras E and Lukin M D 2011 Properties of nitrogen-vacancy centers in diamond: the group theoretic approach *New J. Phys.* **13** 025025
[67] Fu K M C, Santori C, Barclay P E, Rogers L J, Manson N B and Beausoleil R G 2009 Observation of the dynamic Jahn-Teller effect in the excited states of nitrogen-vacancy centers in diamond *Phys. Rev. Lett.* **103** 256404